Crystal Structure of a Murine Glutathione *S*-Transferase in Complex with a Glutathione Conjugate of 4-Hydroxynon-2-enal in One Subunit and Glutathione in the Other: Evidence of Signaling across the Dimer Interface[†,‡]

Bing Xiao,[§] Sharda P. Singh,[||] Bindu Nanduri,[||] Yogesh C. Awasthi,[⊥] Piotr Zimniak,*[,||,#] and Xinhua Ji*[,§]

ABL-Basic Research Program, NCI−Frederick Cancer Research and Development Center, Frederick, Maryland 21702, Departments of Internal Medicine and of Biochemistry & Molecular Biology, University of Arkansas for Medical Sciences, and VA John McClellan Memorial Hospital, Little Rock, Arkansas 72205, and Department of Human Biological Chemistry and Genetics, The University of Texas Medical Branch, Galveston, Texas 77555

Received March 1, 1999; Revised Manuscript Received June 10, 1999

ABSTRACT: mGSTA4-4, a murine glutathione *S*-transferase (GST) exhibiting high activity in conjugating the lipid peroxidation product 4-hydroxynon-2-enal (4-HNE) with glutathione (GSH), was crystallized in complex with the GSH conjugate of 4-HNE (GS-Hna). The structure has been solved at 2.6 Å resolution, which reveals that the active site of one subunit of the dimeric enzyme binds GS-Hna, whereas the other binds GSH. A marked asymmetry between the two subunits is evident. Most noticeable are the differences in the conformation of arginine residues 69 and 15. In all GST structures published previously, the guanidino groups of R69 residues from both subunits stack at the dimer interface and are related by a (pseudo-) 2-fold axis. In the present structure of mGSTA4-4, however, the two R69 side chains point in opposite directions, although their guanidino groups remain in contact. In the subunit with bound GSH, R69 also interacts with R15, and the guanidino group of R15 points away from the active site, whereas in the subunit that binds GS-Hna, R15 pivots into the active site, which breaks its interaction with R69. According to our previous results [Nanduri et al. (1997) *Arch. Biochem. Biophys*. *335*, 305−310], the availability of R15 in the active site assists the conjugation of 4-HNE with GSH. We propose a model for the catalytic mechanism of mGSTA4-4 in conjugating 4-HNE with GSH—i.e., the guanidino group of R15 is available in the active site of only one subunit at any given time and the stacked pair of R69 residues act as a switch that couples the concerted movement of the two R15 side chains. The alternate occupancy of 4-HNE in the two subunits has been confirmed by our kinetic analysis that shows the negative cooperativity of mGSTA4-4 for 4-HNE. Disruption of the signaling between the subunits by mutating the R69 residues released the negative cooperativity with 4-HNE.

4-Hydroxyalkenals are the relatively stable, and thus diffusible, products of membrane lipid peroxidation. Due to their highly electrophilic nature, these compounds can attack various nucleophiles, resulting in cellular dysfunction and toxicity (reviewed in ref *1*). 4-Hydroxynon-2-enal (4-HNE),[1] the major 4-hydroxyalkenal formed during peroxidation of arachidonic and linoleic acids, has been shown to be cytotoxic, cytostatic, genotoxic, and chemotactic (*1*−*8*). The sulfhydryl groups of proteins, and low-molecular-weight thiols such as glutathione (GSH), lysine and histidine residues in proteins, and nucleophilic groups in DNA are potential targets of 4-HNE. Adducts of proteins with 4-HNE have been identified in animals and humans, suggesting the involvement of this lipid peroxidation product in the pathophysiology of degenerative disorders such as atherosclerosis and Parkinson's and Alzheimer's diseases (*9*, *10*). At higher concentrations, 4-HNE causes rapid cell death preceded by multiple pathological processes such as depletion of sulfhydryl groups, disturbances in Ca^{2+} homeostasis, inhibition of critical enzymes, and disruption of protein and DNA synthesis (reviewed in ref *1*). 4-HNE has also been reported to cause the programmed cell death in culture (*11*).

In recent years, numerous studies suggested a role of 4-HNE in cellular signaling (reviewed in ref *12*), generating much interest in the possible physiological functions of

[†] This work was supported by NIH Grants ES07804 (P.Z.) and CA27967 (Y.C.A.) and by the National Cancer Institute, DHHS, under contract with ABL (X.J.). The contents of this publication do not necessarily reflect the views or policies of the DHHS, nor does mention of trade names, commercial products, or organizations imply endorsement by the DHHS or the United States Government.

[‡] The coordinates have been deposited with the Protein Data Bank (accession code 1b48).

* Address correspondence to these authors. X.J.: phone (301) 846-5035; fax (301) 846-6073; e-mail jix@ncifcrf.gov; postal NCI-FCRDC, P.O. Box B, Frederick, MD 21702. P.Z.: phone (501) 257-4843; fax (501) 257-4822; e-mail pxzimniak@life.uams.edu; postal VA Hospital Medical Research (151/LR), 4300 West 7th St., Little Rock, AR 72205.

[§] NCI−Frederick Cancer Research and Development Center.

[||] Department of Internal Medicine, University of Arkansas for Medical Sciences.

[⊥] The University of Texas Medical Branch.

[#] Department of Biochemistry & Molecular Biology, University of Arkansas for Medical Sciences, and VA John McClellan Memorial Hospital.

[1] Abbreviations: GSH, glutathione; GST, glutathione *S*-transferase; xGSTY*m-n*, class Y (A, alpha; M, mu; P, pi; S, sigma) GST with subunit type *m-n* (*m* and *n* = 1, 2, ...) from x (m, murine; h, human; r, rat; s, squid; b, bovine); 4-HNE, 4-hydroxynon-2-enal; GS-Hna, 3-(4-hydroxynonanyl)glutathione, i.e., the product of glutathione conjugation of 4-HNE; CDNB, 1-chloro-2,4-dinitrobenzene; rms, root mean square.

10.1021/bi990468i CCC: $18.00
Published on Web 08/20/1999

4-HNE. At estimated physiological concentrations, 4-HNE can stimulate neutrophil migration (*13, 14*), indicating its involvement in the process of inflammation. Inhibition of proliferation and induction of cell differentiation have been observed in HL-60 cells exposed to estimated physiological concentrations of 4-HNE (*15*). A single treatment of HeLa cells with 0.1−1.0 μM 4-HNE initially decreased the proliferation of these cells, which was followed by enhanced cell growth (*12*). In K562 cells, 1 μM 4-HNE caused the inhibition of ornithine decarboxylase (*15*). Because ornithine decarboxylase is a regulatory enzyme in the polyamine synthesis pathway, 4-HNE might play an important role in cell growth, proliferation, and perhaps differentiation. The effects of 4-HNE on a number of specific regulatory proteins have also been shown. For example, exposure to low levels of 4-HNE caused a transient increase in the activity of adenylyl cyclase (*16*), as well as an increase in basal and GTPγS-induced phospholipase C activity (*17*), in rat liver membranes. On the basis of these and other observations, it has been suggested that 4-HNE acts as a messenger or signal molecule that plays a role in the regulation of cell proliferation and differentiation (*12*).

Because 4-HNE is highly toxic at elevated concentrations (~100 μM) but appears to be involved in cell cycle control and signal transduction at low or "physiological" levels in cells, its concentration must be tightly regulated. The formation of 4-HNE through the lipid peroxidation chain reaction appears to be biologically uncontrollable, because it depends on oxidative stress, which is often caused by exogenous factors (e.g., exposure to xenobiotics) or by imperfect coupling of intracellular redox reactions. Therefore, the major determinant of 4-HNE levels in cells should be its disposition through metabolic pathways. It is therefore important to fully understand the mechanisms of catalysis of 4-HNE-metabolizing enzymes. Even though aldehyde dehydrogenase (*18*) and aldose reductase (*19*) can use 4-HNE as a substrate, the major pathway for disposition of 4-HNE is believed to be GSH conjugation (*20*) catalyzed by a group of glutathione *S*-transferases (GSTs) with exceptionally high activity toward 4-HNE (*21, 22*). Such GSTs have been described in human [hGST 5.8 (*23*) and hGSTA4-4 (24-26), rat [rGST8-8 or rGSTA4-4 (*27*)], bovine [bGST 5.8 (*28*)], and mouse [mGSTA4-4 (*29*)] tissues. We previously cloned the cDNA of mGSTA4-4 (*22*), expressed the protein in *Escherichia coli*, and defined its catalytic properties in relation to 4-HNE and other α,β-unsaturated carbonyl substrates (*29*). Further studies involving site-directed mutagenesis based on the crystal structure of mGSTA4-4 complexed with GSH (*30*) led to a better insight into features of the active site required for high activity toward 4-HNE (*31, 32*). Here, we describe the structure of mGSTA4-4 complexed with a compound relevant to the function of the enzyme—namely, the GSH conjugate of 4-HNE [3-(4-hydroxynonanyl)glutathione (GS-Hna)]—and propose a model for the catalytic mechanism of 4-HNE conjugation by mGSTA4-4.

EXPERIMENTAL PROCEDURES

Materials. Heterologous expression of mGSTA4-4 in *E. coli* and purification of the protein were carried out as previously described (*29*). mGSTA4-4(R69A) and mGSTA4-4(R69C) mutants were obtained by converting the AGG codon encoding R69 to GCG or TGC, respectively, using the QuikChange site-directed mutagenesis kit (Stratagene). The mutant proteins were expressed and purified by the protocol developed for wild-type mGSTA4-4. GS-Hna (Figure 1) was synthesized by incubating 7.8 μmol of 4-HNE with 8.6 μmol of GSH in 2 mL of 50 mM potassium phosphate buffer, pH 7.2, in the presence of 40 μg of mGSTA4-4 for 20 min at 37 °C. The reaction mixture was evaporated to approximately 0.8 mL in a Speedvac and loaded onto a 0.9 × 47 cm Sephadex G-10 column equilibrated with water. The column was eluted with water, and fractions containing GS-Hna were identified by thin-layer chromatography of small aliquots on silica gel plates, using 4:1:1 (v/v/v) 1-butanol:acetic acid:water as the solvent and iodine vapor for visualization. Under these conditions, the R_f of GSH was ~0.1, that of GS-Hna was ~0.4, and that of 4-HNE was ~1.0. Fractions containing GS-Hna were pooled and lyophilized.

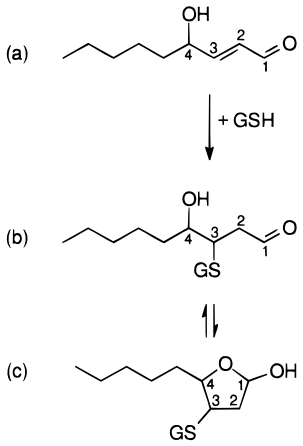

FIGURE 1: Structures of 4-HNE (panel a) and of GS-Hna, the product of conjugation (Michael addition) of 4-HNE with GSH. The open-chain form of GS-Hna is shown in panel b, and the more stable and thus predominant cyclic hemiacetal form (*52*) is shown in panel c.

Crystallization and X-ray Diffraction Data Collection. Crystals of mGSTA4-4·GS-Hna grown under conditions derived from the published protocol (*30*) showed intrinsic disorder. Further crystallization trials were carried out with Hampton crystallization screen kits. The complex was readily crystallized from 36 conditions of Hampton screen kits I and II, producing needlelike crystals. Unfortunately, all of these crystals were either twinned or disordered. The quality of the crystals was improved by using the Hampton additive and detergent screen kits. Single diffraction-quality crystals were grown in hanging drops. First, the complex solution was made by incubation, at 4 °C overnight, of a solution containing 0.3 mM protein, 5 mM GSH, and ~30 mM GS-Hna in 10 mM HEPES buffer (pH 7.5). Second, 4 μL of the complex solution was mixed with 1 μL of ethanol and 6 μL of well solution containing 10% 2-propanol and 12% PEG monomethyl ether 5K in 0.08 M HEPES buffer (pH 7.5). The drops were equilibrated at 19 ± 1 °C. The complex crystallized in the $P2_12_12$ space group with unit cell parameters $a = 114.5$ Å, $b = 96.1$ Å, $c = 50.8$ Å, and $\alpha = \beta = \gamma = 90.0°$. X-ray diffraction data were collected from a single crystal (0.08 × 0.10 × 0.40 mm^3), using a MacScience DIP2020 image plate system with an Enraf Nonius FR 501 rotating anode (45 kV/95 mA) X-ray source.

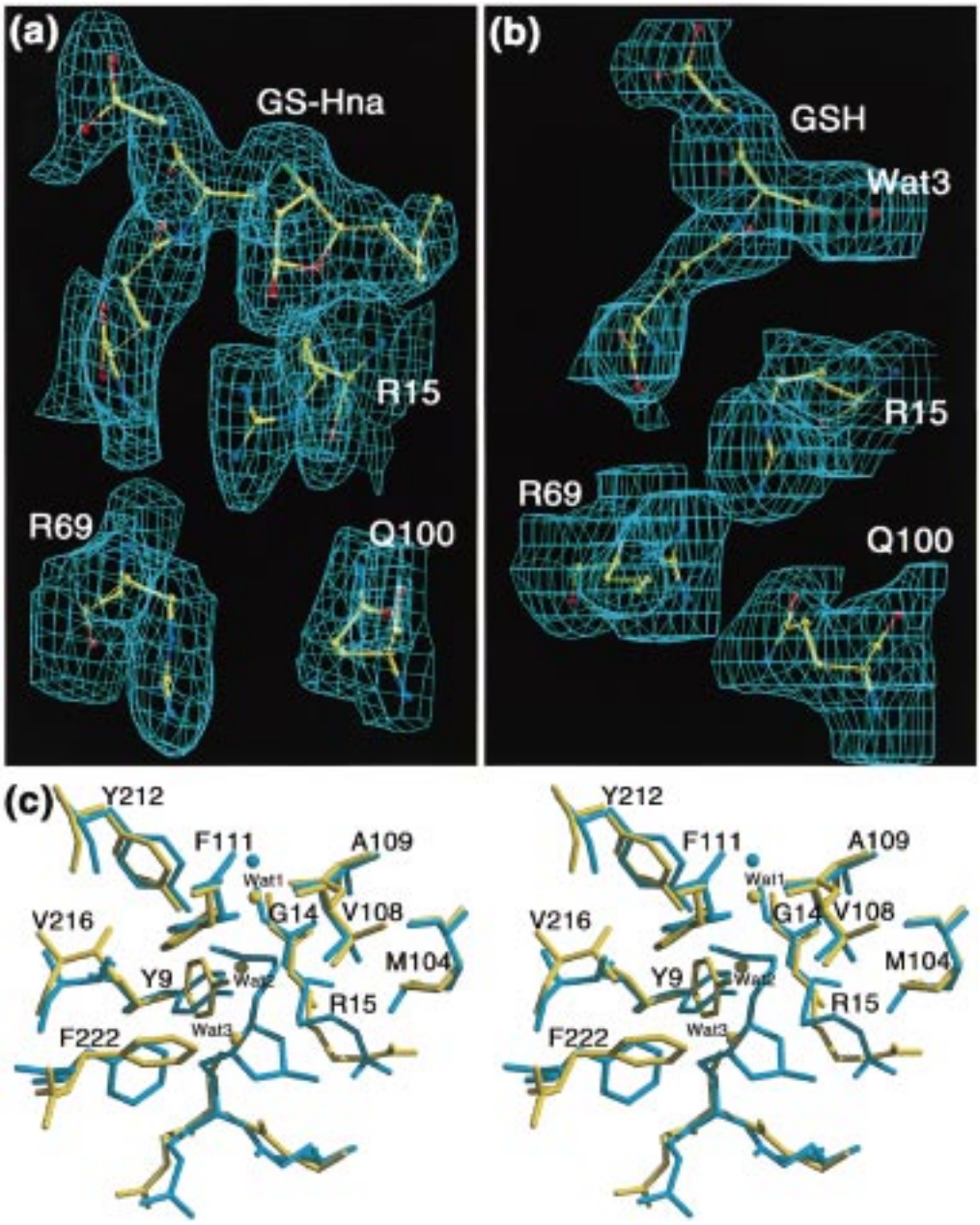

FIGURE 2: Final electron density $2F_o - F_c$ maps, contoured at 1.0σ, of R15, R69, and Q100 with (a) the product molecule GS-Hna and (b) the substrate GSH and a water molecule (Wat3, hydrogen-bonded to the sulfur of GSH) in the complex structure of mGSTA4-4. The side chains and the GS-Hna and GSH molecules are represented by ball-and-stick models with carbon in yellow, oxygen in red, and nitrogen in blue. The electron density is displayed as a cyan net. The xenobiotic substrate-binding site (H-site) residues in the vicinity of the 4-HNE moiety of the two subunits are compared in panel c (stereoview). The subunit containing GS-Hna is in blue and that with GSH is in yellow. The representation was prepared by using O (*38*) and Raster3D (*54*).

The distance between the crystal and detector was 120 mm, and the frame width of the ω scan was 1.0°. The raw data images were processed on a Silicon Graphics Indigo2 computer with a Solid Impact graphics system using the program suite HKL2000 (*33*). Data collection statistics are summarized in Table 1.

Structure Determination and Refinement. The crystal structure of the mGSTA4-4·GS-Hna complex was solved by the molecular replacement technique (*34*) using the program AmoRe (*35*). The search model was the 2.6 Å dimeric structure of hGSTA1-1 (*36*) with the inhibitor removed. Diffraction data from 4 to 10 Å resolution were included for both the rotational and translational searches. The solution was obtained with a correlation coefficient of 0.51 and a crystallographic *R*-factor of 0.45. The molecular replacement solution was used to build a complete model of mGSTA4-4

Table 1: Summary of Data Collection for the Complex of mGSTA4-4 with GS-Hna in One Subunit and with GSH in the Other

X-ray source (rotating anode)	Enraf Nonius FR 591
detector (image plate system)	MacScience DIP 2020
D_{min} (Å)	2.60
redundancy	12.1
overall completeness (%)	87.4
last shell completeness (%)	60.1
overall $I/\sigma(I)$	14.0
last shell $I/\sigma(I)$	2.35
$R_{scaling}$[a]	0.075

[a] $R_{scaling} = \Sigma|I - \langle I\rangle|/\Sigma I$. Friedel pairs were merged.

Table 2: Summary of the Refinement Statistics for the Complex of mGSTA4-4 with GS-Hna in One Subunit and with GSH in the Other

resolution range (Å)[a]	20.0−2.6
no. of reflections used with $I \geq 1\sigma(I)$	15400
crystallographic *R*-factor[b]	0.244
free *R*-value[c]	0.317
no. of amino acid residues	442
no. of substrate/product molecules	1 GSH, 1 GS-Hna
no. of water molecules	40
rms deviations from ideal distances (Å)	
bond distances	0.010
bond angles	0.025

[a] Data used for refinement. [b] The crystallographic *R*-factor $= \sum_{hkl}||F_o| - |F_c||/\sum_{hkl}|F_o|$. [c] Calculated using 5% reflections excluded from crystallographic refinement.

that was refined by using the X-PLOR (*37*) package. The refinement converged when the free *R*-value and the crystallographic *R*-factor, for X-ray diffraction data between 20.0 and 2.6 Å resolution with $I/\sigma(I) \geq 1$, dropped to 0.317 and 0.244, respectively. The GS-Hna molecule was built into the model in two stages. First, GSH was built into the $F_o - F_c$ map contoured at 3σ without any ambiguity. Second, possible diastereomers of the 4-hydroxynonanyl moiety were examined against a difference electron density map contoured at 2σ, among which one was found consistent with the density with two possible conformations. Both conformers were refined for a few rounds and then tested with omit maps, which revealed that only one conformation was correct. The O program suite (*38*) was used on an Indigo2 computer with a Solid Impact graphics system for model building and adjustments. The entire model was checked and adjusted after each cycle of refinement. Strong noncrystallographic restraint was used at the beginning of the refinement. Then the restraint was reduced and finally released as guided by the behavior of the free *R*-values. Water molecules were located in the difference Fourier maps as peaks higher than 3σ. After all the identifiable water molecules were found, the inhibitors and the water molecules were verified by omit maps (*39*). All X-ray diffraction data were included in electron density map calculations. A summary of the crystallographic refinement is found in Table 2. The structure factors and final coordinates have been deposited in the Protein Data Bank under the accession code 1b48.

Enzyme Kinetics. GST activities were measured spectrophotometrically in a 96-well SpectraMax Plus microtiter plate reader (Molecular Devices). Activity with 1-chloro-2,4-dinitrobenzene (CDNB) was measured at 25 °C according to ref *40*, and that with 4-HNE was determined at 30 °C as described in ref *41*. For the determination of kinetic constants, the concentration of 4-HNE was varied between 2.5 and 200 μM in the presence of 0.5 mM GSH. The concentration of CDNB was varied between 0.2 and 2 mM in the presence of 1 mM GSH, and the concentration of GSH was varied between 0.2 and 6 mM in the presence of 1 mM CDNB. Kinetic constants were determined by nonlinear least-squares fitting of the Hill equation to untransformed experimental data using the nonlinear regression module of NCSS 2000 software (Number Cruncher Statistical Systems).

RESULTS AND DISCUSSION

Overall Structure. The final model of the mGSTA4-4 complex includes 442 amino acid residues, 1 GS-Hna, 1 GSH, and 40 water molecules (Table 2). The final electron density maps for GS-Hna and GSH are shown in Figure 2, panels a and b, respectively. Omit maps have similar quality. The crystal structure has good geometry. The root-mean-square (rms) deviations for bond distances and angle distances are 0.010 and 0.025 Å, respectively (Table 2). According to the protein structure verification procedure PROCHECK (*42*), 82% of the residues exhibit the most favorable $\phi-\psi$ relationship. The fold of the polypeptide chain is virtually the same as that reported previously for other known GST structures (*43*). Each subunit contains two domains, a smaller α/β domain and larger α domain. The N-terminal α/β domain contains the secondary-structure elements β2, α1, β1, α2, β3, β4, and α3. The C-terminal α domain consists of six α-helices (α4−α9).

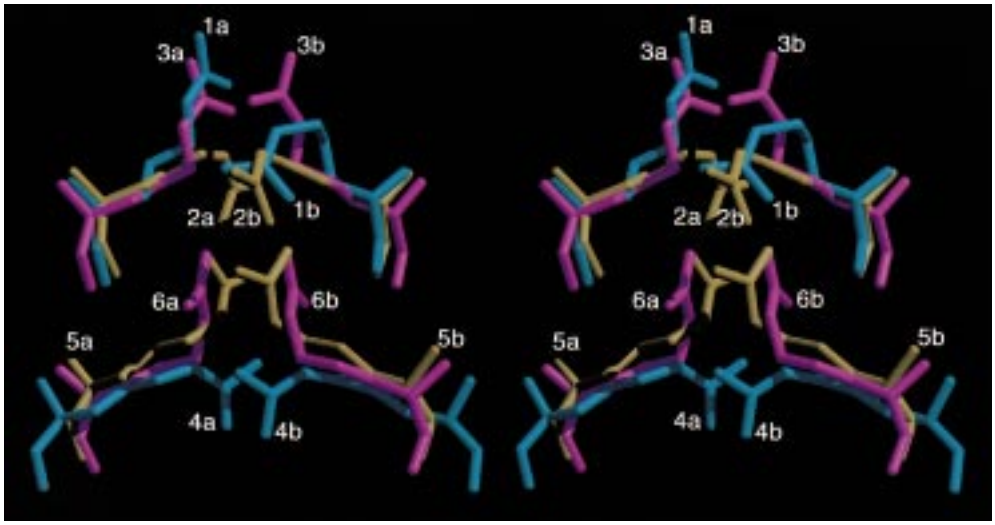

FIGURE 3: Stereoview of the superposition of the "stacking" arginine residues in six GST structures. They are R69 in mGSTA4-4 (1a and 1b, in blue) (this work), R69 in mGSTA4-4 (2a and 2b, in yellow) (*30*), R69 in hGSTA1-1 (3a and 3b, in magenta) (*36*), R77 in rGSTM1-1 (4a and 4b, in blue) (*44*), R70 in pGSTP1-1 (5a and 5b, in yellow) (*55*), and R68 in sGSTS1-1 (6a and 6b, in magenta) (*47*). The relative positions of the stacking arginine residues are the result of the structure-based alignment of dimeric GST structures, using all possible Cα positions. Two clusters have been observed: a cluster for class α enzymes (1, 2, and 3) and that for μ, π, and σ classes (4, 5, and 6). The offset between the two clusters is approximately that of one helical turn. The representation was prepared by using Raster3D (*54*).

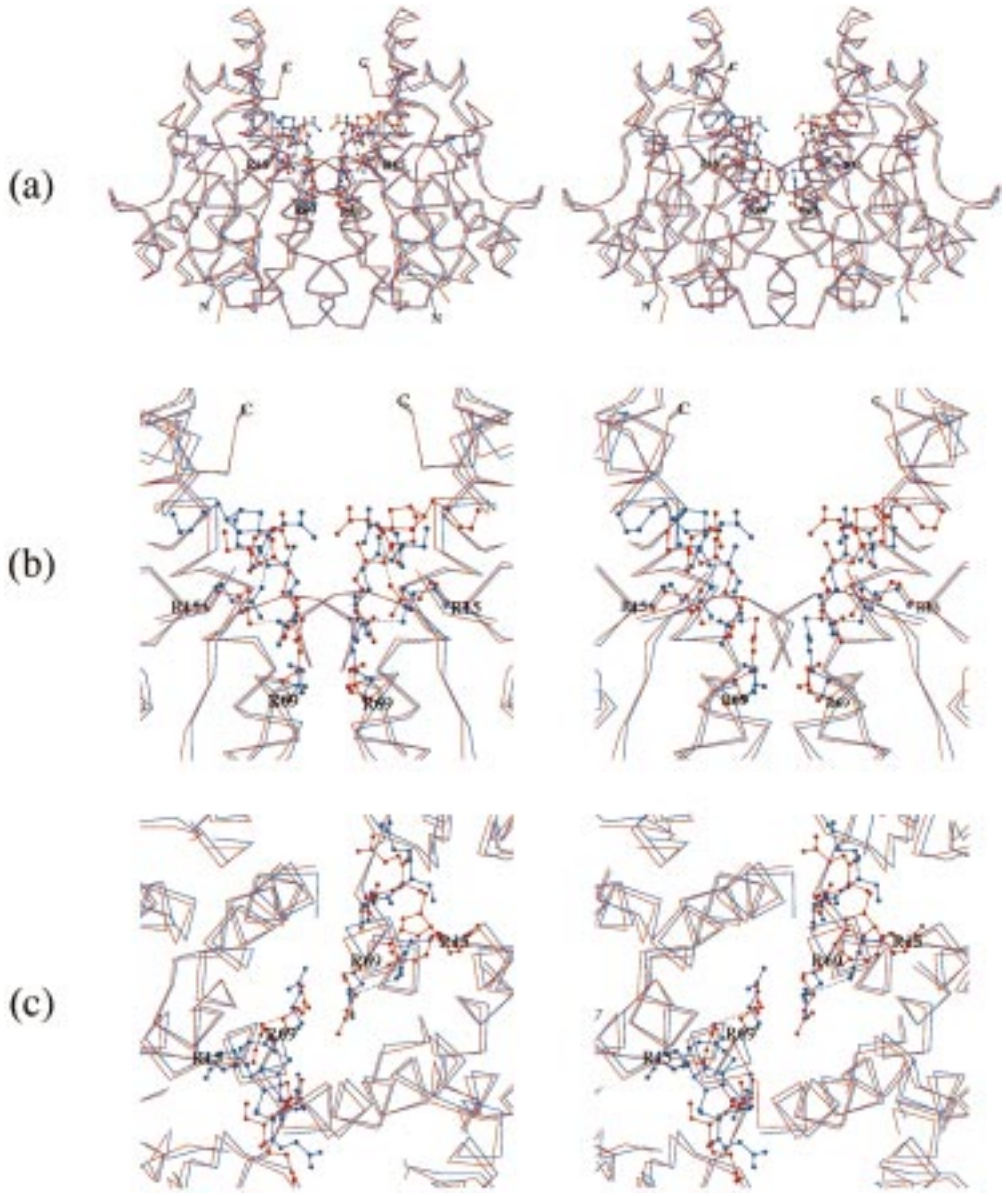

FIGURE 4: Superposition of mGSTA4-4 complex structure (Cα trace in blue) and the resulting structure after a 180° rotation around the pseudo-2-fold axis between the two subunits (Cα trace in red). The view perpendicular to the pseudo-2-fold axis is shown in panel a (overall) and panel b (close-up), and that along the axis is shown in panel c (close-up). The R15 and R69 side chains and the GSH and GS-Hna molecules are shown as ball-and-stick models. Dashed lines indicate electrostatic interactions. The illustration was prepared by using Molscript (*53*).

Subunit−Subunit Interactions. In their biologically active form, cytosolic GSTs are dimeric, and mGSTA4-4 conforms to this rule. Its subunit interface contains the "hydrophobic lock" motif, in which the side chain of either a phenylalanine or a tyrosine residue from one subunit is inserted into a pocket formed by five hydrophobic side chains from the second subunit. The hydrophobic lock is characteristic of the α, μ, π, and Sj GST structures (*44*, *45*) but is incomplete in θ-class GST (*46*) and absent in σ-class GST (*47*). These interface differences, as well as the arginine stacking described below, support the evolutionary scheme proposed by Pemble and Taylor (*48*) and Ji et al. (*47*).

It has been observed that an arginine residue from one subunit stacks with a symmetry-related arginine residue from the second subunit in the α, μ, π, σ, and Sj GST structures (*44*) but not in the θ-class enzymes from *Lucilia cuprina* (*49*) and *Arabidopsis thaliana* (*46*). Two conformations of these stacked arginine side chains have been described, with their guanidino groups pointing in opposite directions (Figure 3). In all GST structures published previously, the two side chains are related by a (pseudo-) 2-fold axis running through the dimer interface. Consequently, the two arginine side chains assume the same conformation in a particular structure. For example, in 1guk (mGSTA4-4) (*30*) and 6gst (rGSTM1-1) (*44*, *50*), the two side chains assume the "down" conformation, whereas in 1guh (hGSTA1-1) (*36*), 1pgt (hGSTP1-1) (*45*), and 1gsq (sGSTS1-1) (*47*), the two adopt the "up" conformation (Figure 3). Although there are minor differences among the various structures, the concordant conformation of the two arginine side chains (i.e., both up or both down) had been consistently found until the current structure determination. In the present structure, one guanidino group points up, whereas the other points down (Figure 3). The asymmetric nature of the dimeric molecule was evident during the refinement. Both the free *R*-value and crystallographic *R*-factor were improved when the noncrys-

tallographic symmetry restraints were weakened and gradually released. To illustrate this asymmetric behavior and its implications, we aligned the structure of the protein−product complex to itself as if the dimeric molecule were rotated around the pseudo-2-fold axis by 180° (Figure 4). Although the two R69 side chains are not symmetric, the two guanidino groups are still stacking with each other with a distance of 4.0 Å between the two groups (Figure 4, panels b and c). The positive charge of R69 is neutralized by D97 in both subunits. The asymmetric behavior of the R69 side chains is likely to be related to the asymmetric occupation of the two active sites (see below).

Protein−Product Interactions. GS-Hna, the product of GSH and 4-HNE conjugation, is found in only one subunit of the mGSTA4-4 dimer, whereas the other subunit has only a GSH molecule in the active site (Figure 4). The product molecule is in its cyclic hemiacetal form (see Figure 1). The part of GS-Hna derived from 4-HNE is oriented so that the five-carbon chain points into the H-site and the hydroxyl group (originating from the aldehydic oxygen atom of 4-HNE) is at a distance of 4.1 Å from NH1 of the guanidino group of R15 (Figure 2c). This proximity suggests a direct interaction between the 4-HNE substrate molecule and R15. It is striking that when the active site is occupied by GSH only, R15 assumes a significantly different conformation, with its guanidino group pointing away from the active site. In both subunits, the interaction of the protein with GSH or the GSH-derived portion of GS-Hna is similar. In both active sites, there is one conserved water molecule (Wat1, Figure 2c). When the H-site is not occupied by the product molecule, two additional water molecules are found in the H-site (Wat2 and Wat3, Figure 2c). Comparison of the subunit with a free H-site with the subunit in which GS-Hna is bound revealed conformational changes for Y9, M104, V108, F111, V216, and F222. The Cα positions of V216 and F222 also shift significantly because they are on the C-terminal helix that forms one wall of the H-site. The global conformational differences with and without the Hna moiety are illustrated in Figure 4. The rms deviation between the two subunits is 0.58 Å for 218 pairs of Cα atoms. The Cα atoms of A2, A3, and E118 are excluded to optimize the alignment.

Possible Role of R15 and R69 in Signaling across the Dimer Interface. We have previously demonstrated that the M104E mutation in mGSTA4-4 leads to a decrease in catalytic efficiency for 4-HNE but not for CDNB, probably due to the formation of a salt bridge between the carboxyl group of E104 and the guanidino group of R15 (*31*). This selective effect of sequestering of R15 on enzyme action indicates that the guanidino group assists in the GSH conjugation of 4-HNE. The mechanism of this assistance remains to be defined but is likely to involve an interaction of R15 with the 4-HNE substrate. In agreement with this model, the present crystal structure shows that R15 points into the active site of the subunit occupied by the substrate (or product) but is turned away from the active site in the subunit occupied by GSH. This is schematically depicted in Figure 5a. The incoming 4-HNE molecule would induce the conformational switch of R15 between the two possible positions described previously (Figure 2). This is shown schematically in subunit B in Figure 5b. Pivoting the R15 side chain into the active site of subunit B would break the interactions of R15 with Q100 and with R69, which are now too far (7.1 and 8.2 Å, respectively) to interact with R15. This appears energetically unfavorable. However, the stacked R69 pair at the subunit interface can switch to its alternative position, which would reestablish the interaction of R15 with R69 and Q100 in the other subunit (subunit A, Figure 5b), provided that R15 in subunit A pivots out of the active site. The latter event is likely to facilitate product (GS-Hna) release from subunit A. In effect, the chain of three arginines previously present in subunit B and the subunit interface is now restored in subunit A and the subunit interface. The enzyme assumes a state (Figure 5c) functionally equivalent to the initial state (Figure 5a), except that the two subunits are reversed with respect to substrate/product binding.

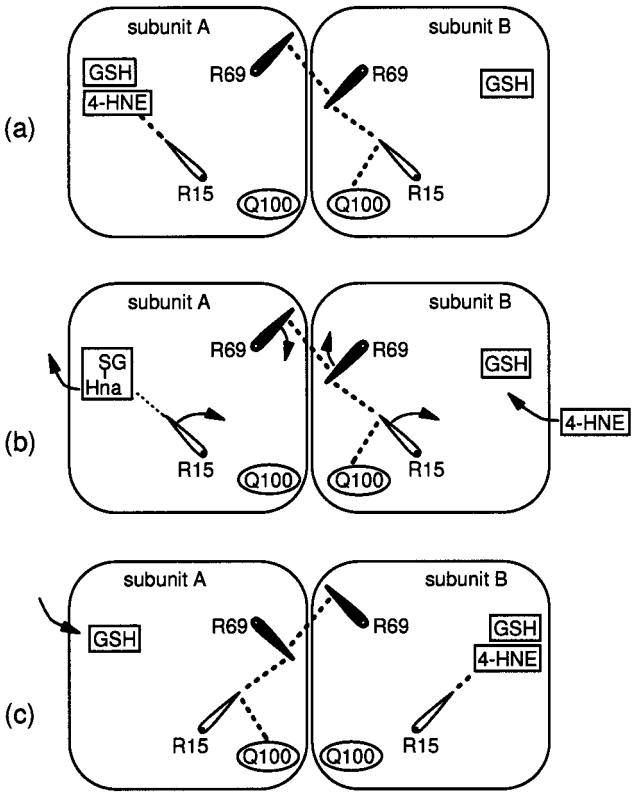

FIGURE 5: Schematic representation of the proposed mechanism of negative cooperativity between mGSTA4-4 subunits during catalysis of 4-HNE conjugation. The side chains of amino acids (R15 and R69 of both subunits) likely to mediate signaling between subunits are depicted. The three panels show consecutive stages of the reaction cycle, with panel b corresponding to the mGSTA4-4−reaction product complex structure. See text for details.

According to the above scheme, a concerted conformational change of the R15 and R69 side chains favors alternate occupancy of the H-sites in the two subunits, i.e., a situation in which, at any given time, only one of the subunits binds 4-HNE (or GS-Hna). The necessary conformational signaling across the dimer interface appears to be caused by the stacked pair of R69 residues, which act like a bipolar switch.

Kinetic Characterization of Enzymes. The model for alternate site occupancy of the subunits by 4-HNE is equivalent to negative cooperativity of the enzyme in the reaction with 4-HNE. Because R15 is not thought to be involved in a direct interaction with CDNB (*31*), the enzyme should conform to Michaelis−Menten kinetics when assayed with CDNB. This was indeed the case. As shown in Table 3, the Hill coefficient with CDNB was statistically not different from 1, demonstrating that the enzyme conforms

Table 3: Kinetic Parameters of Wild-Type mGSTA4-4 and of Mutants of Residue 69[a]

substrate		wild-type mGSTA4-4	mGSTA4-4-(R69A)	mGSTA4-4-(R69C)
4-HNE	k_{cat} (s^{-1})	366 ± 83	194 ± 20	163 ± 6
	K (μM)	205 ± 104	72 ± 12	61 ± 3
	n	0.79 ± 0.10	1.50 ± 0.28	2.03 ± 0.20
CDNB	k_{cat} (s^{-1})	54.4 ± 12.1	28.4 ± 4.2	17.1 ± 15.9
	K (mM)	4.7 ± 1.6	6.1 ± 1.4	10.2 ± 13.6
	n	1.04 ± 0.05	1.00 ± 0.03	0.97 ± 0.11
GSH	k_{cat} (s^{-1})	8.69 ± 0.16	7.50 ± 0.21	
	K (mM)	5.3 ± 2.2	8.2 ± 0.6	not determined
	n	1.10 ± 0.06	1.01 ± 0.06	

[a] Kinetic parameters were estimated by nonlinear regression using the Hill equation $v = V_{max}c^n/(K^n + c^n)$ as the model, and values are given ± asymptotic standard errors of the mean. V_{max} was converted to k_{cat}, assuming a molecular mass of 50 kDa for the dimer. For each determination, 10−16 different substrate concentrations were used, and for each substrate concentration, the activity was measured in 3−10 replicate assays. For 4-HNE, the Hill coefficient n of the wild-type enzyme was statistically different from that of the mGSTA4-4(R69A) ($p = 0.05$) and mGSTA4-4(R69C) ($p = 0.04$) mutants. For CDNB, the Hill coefficients were not different from 1 for all three proteins.

to Michaelis−Menten kinetics with this substrate. In contrast, the Hill coefficient of mGSTA4-4 with 4-HNE was 0.79, indicating a negative cooperativity. A further prediction can be made on the basis of the structure reported here. The central role of the stacked R69 pair in relaying from one subunit to the other the information about H-site occupancy by 4-HNE suggests that signaling could be interrupted by mutating R69 to smaller amino acids unable to interact with each other. This interruption should result in a loss of negative cooperativity for 4-HNE but should have no effect on the Hill coefficient with CDNB. This prediction was confirmed experimentally. In the mGSTA4-4(R69A) and mGSTA4-4(R69C) mutants, the Hill coefficient for 4-HNE increased to 1.50 and 2.03, respectively. Although it is presently not known why the mutants which lost subunit signaling via R69 displayed positive cooperativity, the results clearly show that, in the presence of the stacked R69 pair, negative cooperativity is imposed on the enzyme. In contrast, for CDNB, the Hill coefficients of the wild-type enzyme and both mutants were not different from each other and were equal to 1 (Table 3). These results support our proposed model, in which the stacked R69 pair at the subunit interface couples the movements of the R15 side chains in both subunits. The concerted movements of the R15 residues place the guanidino group of one of them in the H-site of first subunit, whereas in the other subunit R15 is pointing away from the H-site. As shown by kinetic analysis, such an arrangement led to alternate occupancy of the two subunits by 4-HNE but did not affect the independent binding of CDNB to the two active sites. This result indicates that, in addition to its universal role in GSH activation characteristic of α-class GSTs (*51*), in the mGSTA4-4 protein, R15 is likely to be involved in the specific activation of 4-HNE but not of CDNB. This conclusion is consistent with the biochemical data presented by us elsewhere (*31*).

REFERENCES

1. Esterbauer, H., Schaur, R. J., and Zollner, H. (1991) *Free Radical Biol. Med. 11*, 81−128.
2. Eckl, P. M., Ortner, A., and Esterbauer, H. (1993) *Mutat. Res. 290*, 183−192.
3. Schauenstein, E. (1982) in *Free Radicals, Lipid Peroxidation and Cancer* (McBrien, D. C. H., and Slater, T. F., Eds.) pp 159−171, Academic Press, London.
4. Poot, M., Verkerk, A., Koster, J. F., Esterbauer, H., and Jongkind, J. F. (1988) *Mech. Ageing Dev. 43*, 1−9.
5. Griffin, D. S., and Segall, H. J. (1987) *J. Biochem. Toxicol. 2*, 155−167.
6. Brambilla, G., Sciaba, L., Faggin, P., Maura, A., Marinari, U. M., Ferro, M., and Esterbauer, H. (1986) *Mutat. Res. 171*, 169−176.
7. Hauptlorenz, S., Esterbauer, H., Moll, W., Pumpel, R., Schauenstein, E., and Puschendorf, B. (1985) *Biochem. Pharmacol. 34*, 3803−3809.
8. Esterbauer, H. (1982) in *Free Radicals, Lipid Peroxidation and Cancer* (McBrien, D. C. H., and Slater, T. F., Eds.) pp 101−128, Academic Press, London.
9. Yoritaka, A., Hattori, N., Uchida, K., Tanaka, M., Stadtman, E. R., and Mizuno, Y. (1996) *Proc. Natl. Acad. Sci. U.S.A. 93*, 2696−2701.
10. Sayre, L. M., Zelasko, D. A., Harris, P. L. R., Perry, G., Salomon, R. G., and Smith, M. A. (1997) *J. Neurochem. 68*, 2092−2097.
11. Kruman, I., Bruce-Keller, A. J., Bredesen, D., Waeg, G., and Mattson, M. P. (1997) *J. Neurosci. 17*, 5089−5100.
12. Fazio, V. M., Rinaldi, M., Ciafre, S., Barrera, G., and Farace, M. G. (1993) *Mol. Aspects Med. 14*, 217−228.
13. Di Mauro, C., Cavalli, G., Curzio, M., Ferretti, C., Mengozzi, G., Rossi, M. A., Paradisi, L., and Dianzani, M. U. (1995) *Int. J. Tissue React. 17*, 61−72.
14. Curzio, M., Ferretti, C., Stephens, R. J., Esterbauer, H., and Dianzani, M. U. (1994) *Cell Biochem. Funct. 12*, 57−62.
15. Barrera, G., Brossa, O., Fazio, V. M., Farace, M. G., Paradisi, L., Gravela, E., and Dianzani, M. U. (1991) *Free Radical Res. Commun. 14*, 81−89.
16. Paradisi, L., Panagini, C., Parola, M., Barrera, G., and Dianzani, M. U. (1985) *Chem.-Biol. Interact. 53*, 209−217.
17. Rossi, M. A., Fidale, F., Garramone, A., Esterbauer, H., and Dianzani, M. U. (1990) *Biochem. Pharmacol. 39*, 1715−1719.
18. Hartley, D. P., Ruth, J. A., and Petersen, D. R. (1995) *Arch. Biochem. Biophys. 316*, 197−205.
19. Srivastava, S., Chandra, A., Bhatnagar, A., Srivastava, S. K., and Ansari, N. H. (1995) *Biochem. Biophys. Res. Commun. 217*, 741−746.
20. Srivastava, S., Chandra, A., Wang, L. F., Seifert, W. E., Jr., DaGue, B. B., Ansari, N. H., Srivastava, S. K., and Bhatnagar, A. (1998) *J. Biol. Chem. 273*, 10893−10900.
21. Awasthi, Y. C., Zimniak, P., Awasthi, S., Singhal, S. S., Srivastava, S. K., Piper, J. T., Chaubey, M., Petersen, D. R., He, N.-g., Sharma, R., Singh, S. V., Khan, M. F., Ansari, G. A. S., and Boor, P. J. (1996) in *Glutathione S-transferases: Structure, Function and Clinical Implications* (Vermeulen, N. P. E., Mulder, G. J., Nieuwenhuyse, H., Peters, W. H. M., and van Bladeren, P. J., Eds.) pp 111−124, Taylor & Francis, London.
22. Zimniak, P., Eckles, M. A., Saxena, M., and Awasthi, Y. C. (1992) *FEBS Lett. 313*, 173−176.
23. Singhal, S. S., Zimniak, P., Sharma, R., Srivastava, S. K., Awasthi, S., and Awasthi, Y. C. (1994) *Biochim. Biophys. Acta 1204*, 279−286.
24. Hubatsch, I., Ridderstrom, M., and Mannervik, B. (1998) *Biochem. J. 330*, 175−179.
25. Board, P. G. (1998) *Biochem. J. 330*, 827−831.
26. Liu, S., Stoesz, S. P., and Pickett, C. B. (1998) *Arch. Biochem. Biophys. 352*, 306−313.
27. Stenberg, G., Ridderstrom, M., Engstrom, A., Pemble, S. E., and Mannervik, B. (1992) *Biochem. J. 284*, 313−319.
28. Srivastava, S. K., Singhal, S. S., Bajpai, K. K., Chaubey, M., Ansari, N. H., and Awasthi, Y. C. (1994) *Exp. Eye Res. 59*, 151−159.
29. Zimniak, P., Singhal, S. S., Srivastava, S. K., Awasthi, S., Sharma, R., Hayden, J. B., and Awasthi, Y. C. (1994) *J. Biol. Chem. 269*, 992−1000.

30. Krengel, U., Schroter, K. H., Hoier, H., Arkema, A., Kalk, K. H., Zimniak, P., and Dijkstra, B. W. (1998) *FEBS Lett. 422*, 285−290.
31. Nanduri, B., Hayden, J. B., Awasthi, Y. C., and Zimniak, P. (1996) *Arch. Biochem. Biophys. 335*, 305−310.
32. Nanduri, B., and Zimniak, P. (1999) *Arch. Biochem. Biophys. 362*, 167−174.
33. Otwinowski, Z., and Minor, W. (1997) *Methods Enzymol. 276*, 307−326.
34. Rossman, M. G. (1972) *Molecular Replacement Method*, Gordon and Breach, New York.
35. Navaza, J. (1994) *Acta Crystallogr. A50*, 157−163.
36. Sinning, I., Kleywegt, G. J., Cowan, S. W., Reinemer, P., Dirr, H. W., Huber, R., Gilliland, G. L., Armstrong, R. N., Ji, X., Board, P. G., Olin, B., Mannervik, B., and Jones, T. A. (1993) *J. Mol. Biol. 232*, 192−212.
37. Brünger, A. T. (1992) *X-PLOR (3.1): A System for X-ray Crystallography and NMR*, Yale University Press, New Haven, CT.
38. Jones, T. A., Zou, J. Y., Cowan, S. W., and Kjeldgaard, M. (1991) *Acta Crystallogr. A47*, 110−119.
39. Bhat, T. N. (1988) *J. Appl. Crystallogr. 21*, 279−281.
40. Habig, W. H., Pabst, M. J., and Jakoby, W. B. (1974) *J. Biol. Chem. 249*, 7130−7139.
41. Alin, P., Danielson, U. H., and Mannervik, B. (1985) *FEBS Lett. 179*, 267−270.
42. Laskowski, R. A., MacArthur, M. W., Moss, D. S., and Thornton, J. M. (1993) *J. Appl. Crystallogr. 26*, 283−291.
43. Armstrong, R. N. (1997) *Chem. Res. Toxicol. 10*, 2−18.
44. Ji, X., Zhang, P., Armstrong, R. N., and Gilliland, G. L. (1992) *Biochemistry 31*, 10169−10184.
45. Ji, X., Tordova, M., O'Donnell, R., Parsons, J. F., Hayden, J. B., Gilliland, G. L., and Zimniak, P. (1997) *Biochemistry 36*, 9690−9702.
46. Prade, L., Hof, P., and Bieseler, B. (1997) *Biol. Chem. 378*, 317−320.
47. Ji, X., von Rosenvinge, E. C., Johnson, W. W., Tomarev, S. I., Piatigorsky, J., Armstrong, R. N., and Gilliland, G. L. (1995) *Biochemistry 34*, 5317−5328.
48. Pemble, S. E., and Taylor, J. B. (1992) *Biochem. J. 287*, 957−963.
49. Wilce, M. C. J., Board, P. G., Feil, S. C., and Parker, M. W. (1995) *EMBO J. 14*, 2133−2143.
50. Xiao, G., Liu, S., Ji, X., Johnson, W. W., Chen, J., Parsons, J. F., Stevens, W. J., Gilliland, G. L., and Armstrong, R. N. (1996) *Biochemistry 35*, 4753−4765.
51. Bjornestedt, R., Stenberg, G., Widersten, M., Board, P. G., Sinning, I., Jones, T. A., and Mannervik, B. (1995) *J. Mol. Biol. 247*, 765−773.
52. Schauenstein, E., Dorner, F., and Sonnenbichler, J. (1968) *Z. Naturforsch. 23b*, 316−319.
53. Kraulis, P. J. (1991) *J. Appl. Crystallogr. 24*, 946−950.
54. Merritt, E. A., and Bacon, D. J. (1997) *Methods Enzymol. 277*, 505−524.
55. Reinemer, P., Dirr, H. W., Ladenstein, R., Schaffer, J., Gallay, O., and Huber, R. (1991) *EMBO J. 10*, 1997−2005.

BI990468I